

This is an Open Access document downloaded from ORCA, Cardiff University's institutional repository:<https://orca.cardiff.ac.uk/id/eprint/97287/>

This is the author's version of a work that was submitted to / accepted for publication.

Citation for final published version:

Rabizadeh, Taher, Stawski, Tomasz M., Morgan, David John , Peacock, Caroline L. and Benning, Liane G. 2017. The effects of inorganic additives on the nucleation and growth kinetics of calcium sulfate dihydrate crystals. *Crystal Growth and Design* 17 (2) , pp. 582-589. 10.1021/acs.cgd.6b01441

Publishers page: <http://dx.doi.org/10.1021/acs.cgd.6b01441>

Please note:

Changes made as a result of publishing processes such as copy-editing, formatting and page numbers may not be reflected in this version. For the definitive version of this publication, please refer to the published source. You are advised to consult the publisher's version if you wish to cite this paper.

This version is being made available in accordance with publisher policies. See <http://orca.cf.ac.uk/policies.html> for usage policies. Copyright and moral rights for publications made available in ORCA are retained by the copyright holders.



1 **The effects of inorganic additives on the nucleation and growth kinetics of calcium**
2 **sulfate dihydrate crystals**

3
4 Taher Rabizadeh^{1*}, Tomasz M. Stawski², David J. Morgan⁴, Caroline L. Peacock¹, Liane G.
5 Benning^{1,2,3*}

6 1- Cohen Geochemistry Laboratory, School of Earth and Environment, University of Leeds,
7 Leeds, LS2 9JT, United Kingdom

8 2- GFZ, German Research Centre for Geosciences, Telegrafenberg, 14473 Potsdam,
9 Germany

10 3- Department of Earth Sciences, Free University of Berlin, 12249 Berlin, Germany

11 4- Cardiff Catalysis Institute, School of Chemistry, Cardiff University, Cardiff, CF10 3AT,
12 United Kingdom

13
14 * Correspondence to: Taher Rabizadeh (eetr@leeds.ac.uk) and Liane G. Benning
15 (Benning@gfz-potsdam.de)

16
17 **Abstract**

18
19 The effects of 50-500 mmol/L alkali and alkaline earth metal additives (Li^+ , Na^+ , K^+ , Mg^{2+}) on
20 the crystallisation kinetics and mechanisms of calcium sulfate dihydrate (gypsum;
21 $\text{CaSO}_4 \cdot 2\text{H}_2\text{O}$) from supersaturated aqueous solutions were determined by *in situ* and time
22 resolved UV-VIS spectrophotometry. The surface or structural associations between these
23 additives and the end-product gypsum crystals were evaluated through a combination of
24 inductively coupled plasma mass or optical emission spectrometric analyses of digested end-
25 products and X-ray photoelectron spectroscopy (XPS) of the surface composition of the solids.
26 Furthermore, X-ray diffraction (XRD) and scanning electron microscopy (SEM) were utilised

27 for determining any changes in phase composition and morphologies of the formed crystals.
28 Our results revealed that Mg^{2+} , even at low concentrations, decreased the nucleation and
29 growth kinetics 5-10 fold more than Li^+ , Na^+ and K^+ . In all cases, the additives also changed
30 the shapes and sizes of the formed crystals, with Mg^{2+} and Li^+ resulting in longer and thinner
31 crystals compared to the additive-free system. In addition, we showed that, regardless of
32 concentration, Mg^{2+} , Li^+ and K^+ only adsorbed to the newly forming surfaces of the growing
33 gypsum crystals, while ~ 25% of Na^+ became incorporated into the synthesised crystals.

34

35 **Keywords:** crystallisation; calcium sulfate dihydrate; kinetics, surface adsorption; X-ray
36 photoelectron spectroscopy

37

38 **1. Introduction**

39

40 Calcium sulfate dihydrate is one of the main evaporite minerals at Earth surface
41 conditions (Freyer & Voigt, 2003) and it is a crucial mineral phase in many industrial processes,
42 where it is extensively used for construction, medical or agricultural applications (Guan, Ma et
43 al., 2009; Ossario et al., 2014). However, in several industrial processes that rely on water
44 handling systems (e.g., oil and gas production, water desalination; Moghaddasi et al., 2006;
45 Rahardianto et al., 2008), the precipitation of gypsum from the fluids results in its deposition
46 as mineral scales on pipes, filters and heat exchangers. This leads to increased cost and
47 reduction in production efficiency. Thus, it is paramount to quantitatively understand how
48 gypsum forms in such systems, particularly because the effects that aqueous ions present in,
49 for example, formation waters, may have on the crystallisation kinetics and morphology of
50 gypsum are still poorly understood. It is well known that both inorganic (Akyol et al., 2009)
51 and organic additives (e.g., Hoang et al., 2011; Rabizadeh et al., 2014) affect the nucleation,

52 crystallisation and morphologies of gypsum crystals. To date primarily the role that trace
53 elements like Cr^{3+} , Cu^{3+} , Al^{3+} and Fe^{3+} have on gypsum growth from solution Hamdona and
54 Al Hadad, 2007; Hasson et al., 1990; Kruger et al., 2001; Sayan et al., 2007; Yang et al., 2009
55 have been studied. In contrast, the effect of major ions in, for example, brines or formation
56 water fluids (e.g., Na^+ , K^+ , Li^+ , Cl^- or Mg^{2+}) are far less understood. Furthermore, existing data
57 from studies that address the crystallisation of calcium sulfate phases in the presence of these
58 ions are highly discrepant and whether these ions become structurally incorporated or only
59 surface adsorbed into the growing gypsum is still debated. For example, Na^+ has been shown
60 to incorporate into the calcium sulphate hemihydrate ($\text{CaSO}_4 \cdot 0.5 \text{H}_2\text{O}$; bassanite; Mao et al.,
61 2014) but not into gypsum (Ben Ahmed et al., 2014). On the other hand, Mg^{2+} was suggested
62 to only incorporate into gypsum (Ben Ahmed et al., 2014). However, lacking so far is a
63 quantitative and molecular level understanding of the processes that lead either to these ions
64 becoming adsorbed onto or incorporated into growing gypsum crystal structures. Lacking is
65 also a mechanistic pathway explaining the role that these crucial ions in brines have on the
66 nucleation, growth and crystallisation of gypsum.

67 To fill this gap we have in this work elucidated the effects that variable concentrations
68 (0-500 mmol/L) of aqueous Li^+ , Na^+ , K^+ and Mg^{2+} ions have on the nucleation and growth
69 kinetics, as well as the morphology of gypsum forming from supersaturated aqueous solutions.
70 We followed the processes by combining analyses of the solution and solids. We determined
71 the mechanisms that control the way these alkali and alkaline earth cations became associated
72 with growing gypsum crystals. We show, in contrast with previously published data, that Li^+ ,
73 K^+ and Mg^{2+} do not incorporate at all into the forming gypsum structures while Na^+ became
74 partly incorporated but still the majority became adsorbed to growing gypsum crystals.
75 However, the major effect that all ions have is in delaying the nucleation and growth through

76 adsorption onto the growing mineral surfaces. In the case of Mg^{2+} and Li^+ this interaction also
77 leads to a change in the resulting crystal morphologies.

78

79 **2. Experimental methods**

80

81 Calcium and sulfate stock solutions were prepared from dissolving analytical grade
82 $CaCl_2 \cdot 2H_2O$ ($\geq 99-100\%$; AnalaR Normapour; VWR) and diluting concentrated H_2SO_4 (93-
83 98% v/vol, AnalaR Normapour; VWR) in $18\text{ M}\Omega\text{cm}^{-1}$ ultra-pure Milli-Q water to reach
84 concentrations of 200 mmol/L. The effects of inorganic metal ions on gypsum crystallisation
85 were evaluated by adding Li^+ , Na^+ , K^+ and Mg^{2+} to separate $CaCl_2 \cdot 2H_2O$ stock solutions, using
86 analytical grade LiCl (puriss. p.a., anhydrous, $\geq 99.0\%$; Sigma-Aldrich), NaCl ($\geq 99.9\%$;
87 Fisher), KCl (puriss. p.a., anhydrous, $\geq 99-100\%$; Sigma-Aldrich) and $MgCl_2 \cdot 6H_2O$ ($\geq 99-$
88 100% ; AnalaR Normapour; VWR). Precipitates were produced by mixing 1 ml of $CaCl_2 \cdot 2H_2O$
89 with or without the additives with 1 ml H_2SO_4 in 4 ml polystyrene cuvettes at room temperature
90 ($21\text{ }^\circ\text{C}$) and under constant stirring. The mixing led to a solution with a pH of ~ 2 and initial
91 $[Ca^{2+}]$ and $[SO_4^{2-}]$ concentrations of 100 mmol/L. The initial concentration of additives in the
92 crystallisation solutions (after mixing) was varied between 50 and 500 mmol/L. Once mixed,
93 all solutions were supersaturated with respect to gypsum as indicated by the saturation indices
94 (as the logarithm of the ion activity product over the solubility product) calculated with the
95 geochemical computer code PhreeqC 3.3.3 and using the Pitzer database (Parkhurst and
96 Appelo, 1999).

97 Changes in the mixed solutions were monitored by measuring the increase in absorbance
98 using a UV-VIS spectrophotometer (Uvikon XL) at $\lambda = 520\text{ nm}$ with an angle between the
99 incident beam and detector of 180° . The reactions were followed at room temperature for up to
100 200 minutes with UV-VIS data collected every second and each experimental set was carried

101 out in triplicate. The absorbance data is plotted as the normalized change in solution turbidity.
102 At the end of each turbidity experiment, the contents of each cuvette were vacuum filtered
103 through 0.2 μm polycarbonate filters, dried and preserved for further analyses (for additional
104 details see Supplementary information Fig. S1).

105 In all experiments, regardless if additives were present or not, the solid end-products
106 were always gypsum as determined by powder X-ray diffraction (XRD; Bruker D8
107 diffractometer; $\text{CuK}\alpha 1$; 2θ range 5 - 35°; resolution 0.105° / step; counting time 1s / step) with
108 XRD patterns analysed with the EVA software (version 3) and the PDF-2-1996 database (see
109 Fig. S2). To accurately determine the d-spacing in all samples, each gypsum end-product
110 powder was mixed with a silicon standard reference material prior to XRD analysis.

111 The morphologies of the resulting gypsum crystals were imaged using a field emission
112 gun scanning electron microscope (FEG-SEM, FEI Quanta 650, 5 kV) and the dimensions of
113 the crystals were evaluated by measuring the lengths and widths of 200 crystals in each sample
114 using the ImageJ v. 1.49 software Abramoff et al., 2004.

115 To evaluate the association between the additives and the formed gypsum, aliquots of
116 the precipitated end-products were dissolved in 2% nitric acid (69% AnalaR NORMAPUR
117 analytical reagent) and the resulting solutions analysed for their Na, Mg, Li, K and Ca contents
118 by inductively coupled plasma mass spectrometry (ICP-MS; Thermo Scientific iCAPQc) and
119 inductively coupled plasma optical emission spectrometer (ICP-OES; Thermo Scientific iCAP
120 7400); for limit of detection and uncertainties see table S1). To differentiate between the
121 potentially surface adsorbed and the structurally incorporated fractions of the additives,
122 aliquots of the end-product gypsum samples were first rinsed 6 times with a saturated gypsum
123 solution to desorb any potentially surface adsorbed additives. The saturated gypsum solution
124 was prepared by equilibrating gypsum (puriss, 99.0-101.0%, Sigma-Aldrich) in 18 $\text{M}\Omega\text{cm}^{-1}$
125 ultra-pure Milli-Q water at pH 2 for 24 hours and filtering through 0.2 μm syringe filters prior

126 to desorption. After this desorption step the remaining solids were digested in 2% nitric acid
127 and the digestion solutions were analysed as described above. The concentrations of additives
128 associated with the end-product gypsum crystals (association amount; C_A) before and after
129 desorption were calculated from the moles of cation measured in the full digestion solution
130 divided by the moles of total dissolved gypsum crystals.

131 Finally, to determine the nature of the surface interactions between the various ions and
132 the formed precipitates, we employed X-ray photoelectron spectroscopy (XPS) with a detection
133 limit of 0.1 at.% (which is roughly 1ppth or 10^{19} atoms/cm³). On both the as-formed and the
134 desorbed end-product solids, XPS was used to determine whether and how metal ions were
135 associated with the mineral surfaces or the crystal structures. XPS spectra were acquired from
136 the top 8-10 nm of end-product gypsum crystals using a Kratos Axis Ultra-DLD spectrometer
137 with a monochromatic Al K_α X-ray source (144 W) and analyser pass energies of either 160
138 eV (survey scans) or 40 eV (high resolution scans). The base pressure during analysis was ca.
139 5×10^{-9} Torr. All data were referenced to the C (1s) signal of adventitious carbon at 284.8 eV
140 and quantified as atomic percentage using CasaXPS™ (Version 2.3.15) using elemental
141 sensitivity factors supplied by the manufacturer.

142

143 **3. Results**

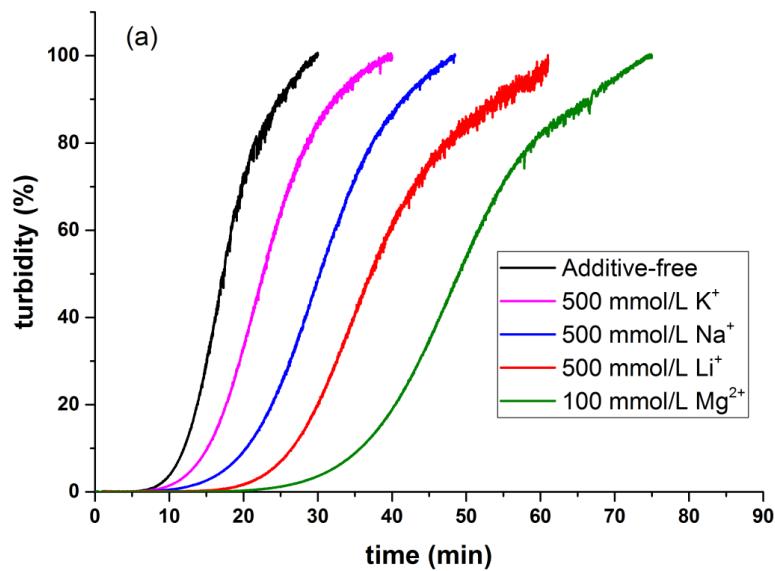
144

145 **3.1. The effects of additives on the crystallisation process**

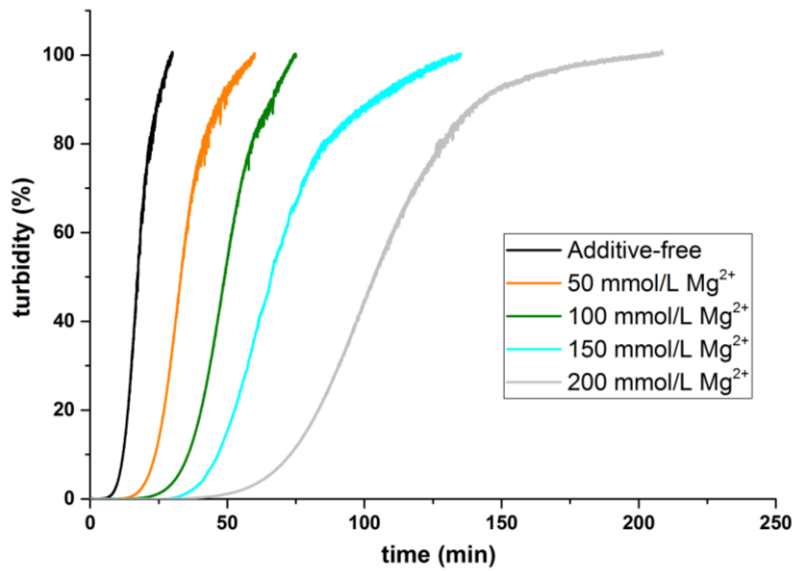
146

147 In the additive-free experiments, the turbidity started to develop after 3 ± 1 minutes (induction
148 time) and it took ~ 30 minutes for the turbidity to reach a steady value on a plateau (Fig 1a,
149 black line). In contrast, in each of the additive-containing experiments (Fig. 1a and b), the
150 induction times and the time to reach a plateau were markedly longer. At the highest

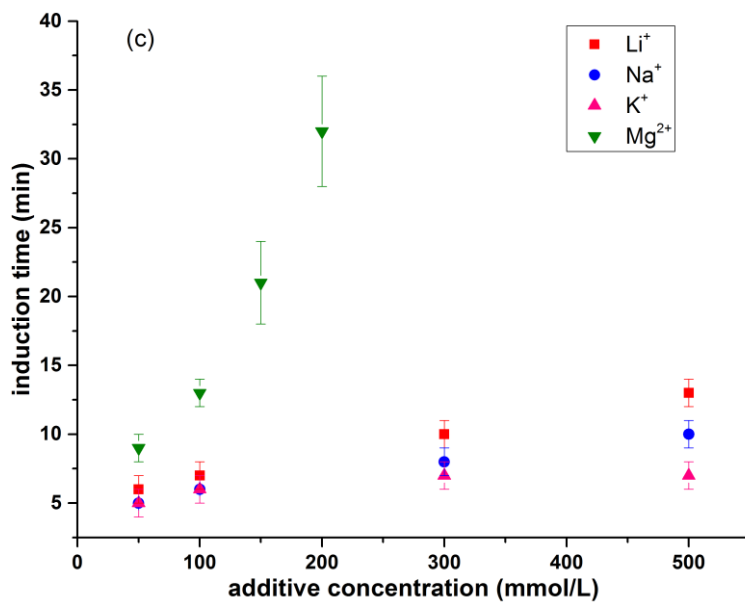
151 concentration (500 mmol/L) of monovalent cations (Li^+ , Na^+ and K^+), the induction time
152 increased in the order $\text{K}^+ < \text{Na}^+ < \text{Li}^+$ by 2 fold, 4 fold and almost 5 fold, respectively (Table
153 S2). The slope of the turbidity decreased and the crystallisation end-plateaus were reached
154 significantly later than in the additive free system in the same order ($\text{K}^+ \sim 37$ min, $\text{Na}^+ \sim 48$
155 min and $\text{Li}^+ \sim 60$ min; Fig. 1a). The turbidity development was even more affected by the
156 presences of Mg^{2+} . Even at a low additive concentration (e.g., 100 mmol/L; Fig 1a) the
157 induction time much longer than for all monovalent cations at 500 mmol/L. Quadrupling the
158 Mg^{2+} concentration from 50 mmol/L to 200 mmol/L, increased the induction time
159 exponentially; Fig. 1b, Table S2). Furthermore, for Mg^{2+} at 300 and 500 mmol/L even after
160 200 minutes of reaction no change in turbidity was observed indicating total inhibition of the
161 reaction under these experimental conditions. For all additives with increasing cation
162 concentrations the induction time increased in linearly (Fig. 1c), but the effect was markedly
163 larger for the divalent Mg^{2+} compared to the monovalent Li^+ , Na^+ and K^+ (Fig. 1c).



164



165



166

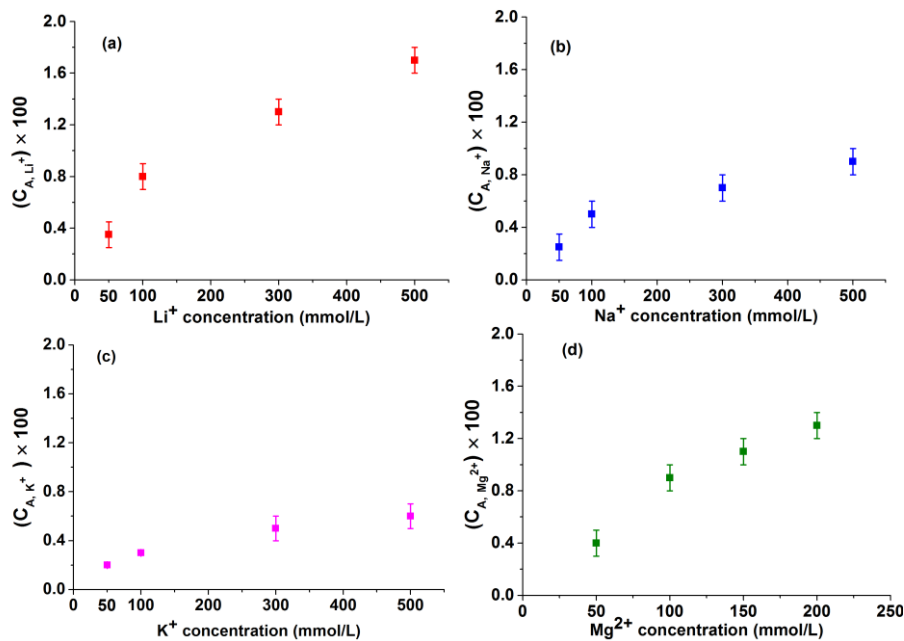
167 Fig. 1. Turbidity curves plotted as a function of time (a) in the absence and presence of high
 168 concentrations of additives (note that Mg²⁺ is only 100 mmol/L while all monovalent ions are 500 mmol/l) ; (b)
 169 at variable concentrations of Mg²⁺; (c) changes in induction times as a function of additive concentrations.

170

171 **3.2 The association between additives and gypsum crystals**

172

173 For all additive ions, increasing additive concentration in solution was mirrored by an
 174 increase in associated ion concentration (C_A) in the solids formed (Fig. 2a-d). For example, for
 175 monovalent additive concentrations between 50 and 500 mmol/L, $C_{A\text{Li}^+}$ increased ~ 5 times,
 176 while $C_{A\text{Na}^+}$ and $C_{A\text{K}^+}$ increased ~ 3 times (Fig. 2a-c). For Mg^{2+} at concentrations up to 200
 177 mmol/L, the $C_{A\text{Mg}^{2+}}$ increased ~ 4 times (Fig. 2d) and reached a value almost equivalent to the
 178 highest value obtained for the C_A of Li^+ at 500 mmol/l. Comparing the association amounts at
 179 a fixed additive concentration (100 mmol/L), mirrors the trend observed for the increase in
 180 induction time, namely $\text{K}^+ < \text{Na}^+ < \text{Li}^+ < \text{Mg}^{2+}$.



181

182 Fig. 2. Variations in cation association at different concentrations of (a) Li^+ (b) Na^+ (c) K^+ (d) Mg^{2+} ;
 183 the error bars represent the standard deviations measured in five replicate samples.

184

185

186

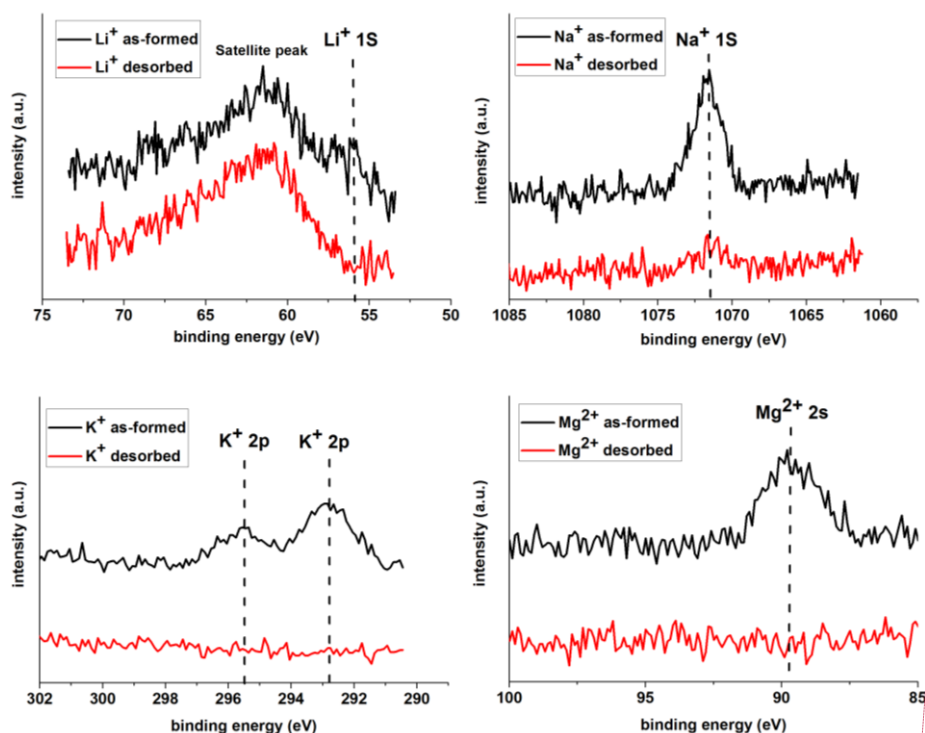
187 When we evaluated the partitioning of additives between crystal surfaces (adsorption)
188 or crystal matrixes (structural incorporation), our data revealed that the C_A for Li^+ , K^+ and Mg^{2+}
189 in the post desorption digested samples were below detection limits. This clearly indicated that
190 these cations were only adsorbed to the surfaces of the growing gypsum crystals with
191 insignificant or no incorporation into the crystal structures. In contrast, at the highest additive
192 concentrations (500 mmol/L), up to 25% of the associated Na^+ ($C_{A\ 500\text{mmol/L}} = 0.002$ out of
193 0.009) became incorporated into the gypsum structure (Fig S3). The additive ion adsorption
194 was also confirmed by XPS surface analyses of as-formed and desorbed gypsum crystals (Fig.
195 3) The XPS spectra confirmed that the Li 1s (55.8 eV), K 2p_{3/2} (292.9 eV) and Mg 2s (89.8
196 eV) peaks were present in all as-formed samples but absent in the post-desorbed samples
197 confirming that these ions were solely surface adsorbed and not incorporated into the gypsum
198 structure (Fig. 3a, c and d). On the other hand, for Na^+ the 1s peak at 1071.64 eV was present
199 in both the as-formed and desorbed gypsum spectra, again corroborating our C_A data (Fig. 3b)
200 that a fraction of the associated Na^+ became sequestered into the gypsum crystal structure. The
201 surface elemental compositions (in atomic percentage) of the as-produced and desorbed
202 gypsum crystals illustrated that Li^+ had the adsorption affinity (1.52 at. %) followed by Mg^{2+}
203 (1.06 at. %), Na^+ (0.34 at. %) and K^+ (0.41 at. %) (Table 1). However, unlike Li^+ , K^+ and Mg^{2+} ,
204 Na^+ remained associated with the gypsum crystals post desorption (0.14 at. %) confirming its
205 structural incorporation. Note the signal of lithium is low due to the small ionisation cross-
206 section of the metal, however the presence of Li can be detected by subtraction of the satellite
207 structure noted in fig 3.

208 Together with the adsorbed ions, in all as-formed but not the desorbed samples, the
209 XPS spectra revealed the presence of Cl^- 2p_{3/2} peaks confirming that Cl^- also became co-
210 adsorbed to the gypsum surfaces (Fig. S4). Furthermore, the Ca to S atomic % ratio was close

Commented [DM1]: Only quote to 1dp as we used 0.1 eV steps

Commented [DM2]: What do we know about the dispersion of these elements? XPS concentrations can be influenced by dispersion – e.g. the smaller the particles and more well dispersed they are then the higher the apparent concentration

211 to 1:1 but the O to Ca or S ratio was higher than 4:1, likely related to gypsum structural water
 212 (Table 1).



213

214 Fig. 3. XPS spectra for the as-formed and desorbed gypsum crystals containing additive
 215 cations. Note that the peak intensities are in arbitrary units and do not represent the
 216 concentration of the elements on the surface.

217 Table 1. Surface composition of the precipitated gypsum crystals detected by XPS (at. %)

	Ca	S	O	Li	Na	K	Mg	Cl	C
Additive-free (as-formed)	11.51	12.01	58.34	-	-	-	-	-	18.14
Additive-free (desorbed)	11.56	12.04	58.29	-	-	-	-	-	18.12
Li ⁺ -500 mmol/L (as-formed)	9.59	9.98	52.34	1.52	-	-	-	1.77	24.80
Li ⁺ -500 mmol/L (desorbed)	12.00	12.66	57.28	-	-	-	-	-	18.06
Na ⁺ -500 mmol/L (as-formed)	12.60	13.08	59.54	-	0.48	-	-	0.05	14.32
Na ⁺ -500 mmol/L (desorbed)	12.32	12.98	59.35	-	0.14	-	-	-	15.13
K ⁺ -500 mmol/L (as-formed)	12.15	12.65	58.79	-	-	0.41	-	0.08	15.63
K ⁺ -500 mmol/L (desorbed)	12.31	13.07	59.86	-	-	-	-	-	14.76

Commented [DM3]: Make swure the S of 1S, P of 2p etc is lowercase

Commented [DM4]: Again quote to 1dp concentration wise

Mg ²⁺ -200 mmol/L (as-formed)	10.21	10.85	48.92	-	-	-	1.06	0.95	28.00
Mg ²⁺ -200 mmol/L (desorbed)	12.25	12.87	57.94	-	-	-	-	-	16.94

3.3. The effects of additives on the morphology of gypsum

Micrographs of the formed gypsum crystals revealed that in the additive-free system, short (4-6 μm) and thin (2-2.5 μm) gypsum crystals formed (Fig. 4a, 5a,b and S6a,b). In contrast, the crystals from the additive-containing solutions were markedly longer and narrower (Fig. 4b, 5b, S6a,b). For example, in the presence of 500 mmol/L Li⁺ the end-product gypsum crystals were ~200% longer and ~50% narrower compared with the additive free crystals.

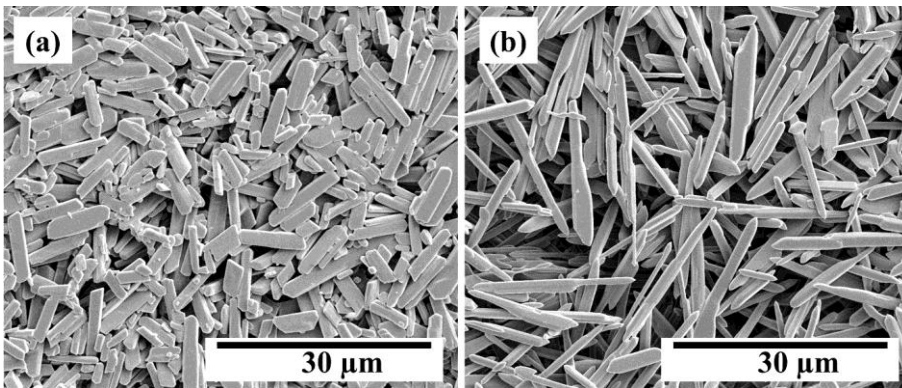
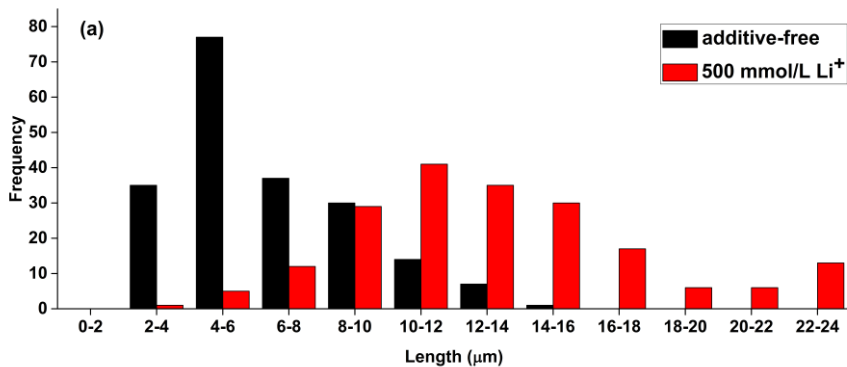


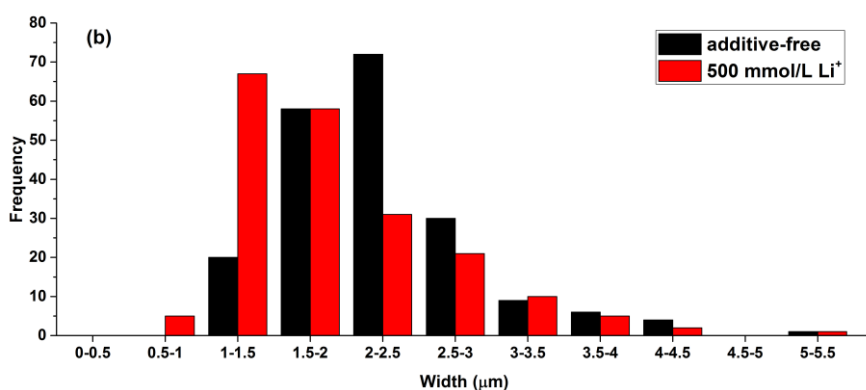
Fig. 4. SEM micrograph of the end-product gypsum crystals in (a) the additive-free system; (b) the presence of 500 mmol/L Li⁺ (for morphologies of gypsum crystals precipitated in the presence of K⁺, Na⁺ and Mg²⁺ see Figs S5).

This is clearly visible in the gypsum crystals grown in the presence of Li⁺ and Mg²⁺ where the length of the resulting crystals was almost double, while the widths slightly decreases compared to the additive-free system (Fig. 5a,b and Figs S6a,b).



234

235



236

237

238

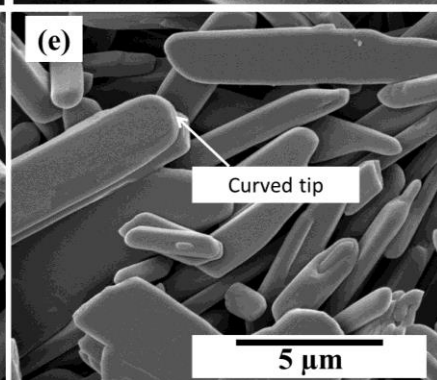
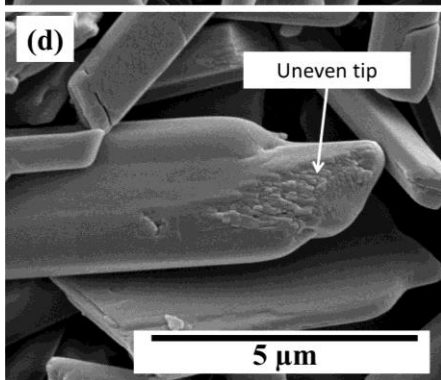
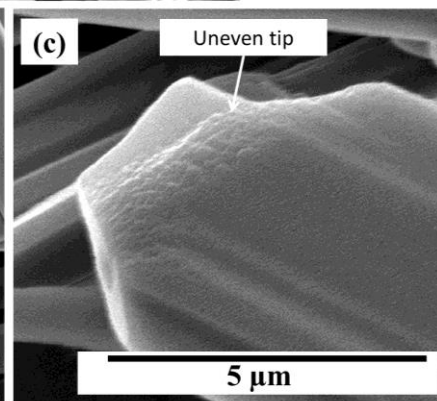
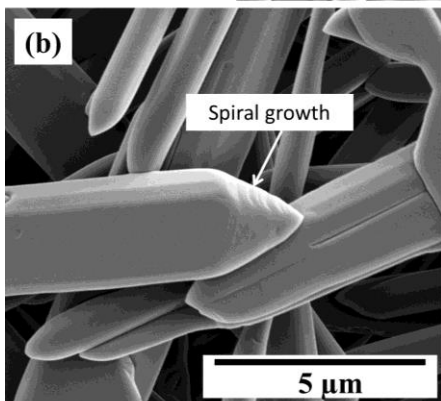
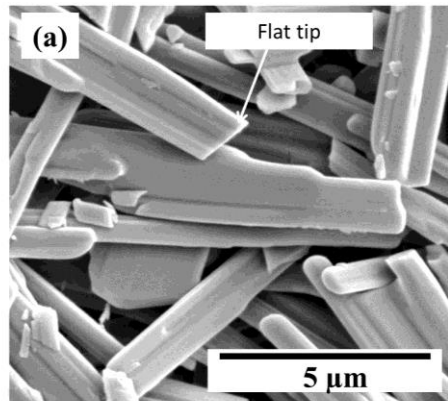
239 Fig. 5. Particle size analysis of gypsum crystals precipitated from solution containing 500
 240 mmol/L Li⁺ after 200 min (a) length of the crystals; (b) width of the crystals (the particles size
 241 analysis of the gypsum crystals precipitated in the presence of 500 mmol/L K⁺, 500 mmol/L
 242 Na⁺ and 200 mmol/L Mg²⁺ are in the supporting information Fig. S6a, b).
 243

244 In addition, the tips of the growing gypsum crystals differed (Fig. 6a-e; S7-10), with the
 245 additive-free crystals having flat tips. For example, in the presence of Li⁺ the tips were broader
 246 and thicker and in these crystals spiral growth and macro-steps were also obvious (Fig. 6a-e
 247 and Fig S7a-c). Similarly, the gypsum crystals precipitated in the presence of 500 mmol/L Na⁺

248 (Fig. 6c and Fig. S8) and K^+ (Fig. 6d and Fig. S9) had uneven tips with micro-steps while the

249 Mg^{2+} modified gypsum crystals had curved tips (Fig. 6e and Fig. S10).

250



251

252 Fig. 6. SEM micrograph of end-product gypsum tips from systems with (a) no additive; (b) 500
253 mmol/L Li⁺ (c) 500 mmol/L Na⁺ (d) 500 mmol/L K⁺ (e) 200 mmol/L Mg²⁺.
254

255 **4. Discussion**

256

257 **4.1. Crystallisation kinetics: role of additives**

258

259 We used the change in turbidity induction times in the absence and presence of the additives
260 as a proxy to evaluate the effects they have on the nucleation and growth of gypsum. Our data
261 showed a clear increase in induction time with increasing additive concentrations, and a
262 decreased in nucleation and growth kinetics in the order K⁺ < Na⁺ < Li⁺ < Mg²⁺ (Figs. 1a-c).
263 Therefore, it is important to assess if the additives also affected the nucleation and growth
264 mechanisms.

265 The increase in ionic strength (IS) with increasing the additive concentrations from 50
266 mmol/L to 500 mmol/L metal invariably resulted in a decrease in the activities of SO₄²⁻ and
267 Ca²⁺ and this affected the solubility of gypsum and delayed precipitation (Fig. 1a-c). This is a
268 well-known process in the CaSO₄ system Sun et al., 2015; Sverjensky et al., 1997; Tanji, 1969;
269 Zhang et al., 2013. Specially, at high additive ion concentrations, and thus high ionic strengths
270 (IS = 1 mol/L and 0.716 mol/L for 500 mmol/L monovalent cations and 200 mmol/L Mg²⁺
271 containing solutions, respectively), for example SO₄²⁻ can be present as ion pairs or charged
272 complexes with sodium (Jiang et al., 2013). Such complexes further decrease the activity of
273 free SO₄²⁻ and CaSO₄⁰ ion pairs. In our study, the additive-sulfate ion-pairing strength increased
274 in the order of K⁺ < Na⁺ < Li⁺ < Mg²⁺ ([KSO₄]⁻ < [NaSO₄]⁻ < [LiSO₄]⁻ < [MgSO₄]⁰) Elgquist
275 and Wedborg, 1978; Jiang et al., 2013; Leaist and Goldik, 2001; Reardon, 1975. As such this
276 likely explains our observation that Mg²⁺ decreased the nucleation rate and increased the
277 solubility of the gypsum crystals more than the monovalent cations. However, it is important

278 to note that the observed order in which these ions affected the induction time and
279 crystallisation kinetics ($K^+ < Na^+ < Li^+ < Mg^{2+}$) is different to what was predicted from the
280 saturation indices calculated by PhreeqC ($Na^+ < Li^+ < K^+ < Mg^{2+}$; Table S3). This indicates that
281 the solubility data in the presence of these ions in the databases (specially for monovalent ions)
282 may need to be re-measured.

283 Once nucleation is overcome, most often the rate-limiting step for crystal growth is
284 determined by cation desolvation (Dove and Czank, 1995). The increase in hydration enthalpy
285 for $K^+ < Na^+ < Li^+ < Ca^{2+} < Mg^{2+}$ reveals that in our system the divalent Mg^{2+} ion (a *chaotrope*)
286 with the highest hydration enthalpy and water residence time Kerisit and Parker, 2004, by far
287 outcompetes the monovalent ions as it limits crystal growth more effectively. Among the
288 monovalent ions, Li^+ (a *chaotrope*) retained its water longer than Na^+ and K^+ (*kosmotropes*)
289 (Sakuma and Kawamura, 2011).

290 This is similar to the inhibitory order for the precipitation of calcium oxalate
291 monohydrate as shown by Farmanesh et al., (2015) or for barium sulfate Kowacz et al., (2007).

292

293 **4.2. Surface adsorption and/or structural incorporation**

294

295 Our results (Fig. 2, 3 and S3) revealed that all the tested inorganic additives adsorbed onto the
296 surfaces of the gypsum crystals and that among them the cations with more negative hydration
297 enthalpies (Li^+ and Mg^{2+}) had the highest surface adsorption affinity (Table 1). This behaviour
298 can be explained by the water “structure making-structure breaking” model (Gierst et al.,
299 1966). According this model, an ion and a surface exerting similar structural effects on their
300 surrounding water, are attracted entropically to each other. Gypsum has a negative heat of
301 immersion (Singh and Middendorf, 2007), thus, Li^+ and Mg^{2+} will bind stronger to its surface
302 compared to Na^+ and K^+ . In addition, equal adsorption (in atomic percentage) of Mg^{2+} and Li^+

303 (Table 1) despite the more than 2 fold lower concentration of Mg^{2+} (200 mmol/L) than Li^+ (500
304 mmol/L) further supports this mechanism. Similar behaviours (i.e., higher surface adsorption
305 of Li^+ than Na^+ and K^+) has been reported for TiO_2 Bourikas et al., 2001, $\alpha-Al_2O_3$ Johnson et
306 al., 1999.

307 Our data (Table 1 and Fig. S4) also showed a high adsorption affinity of Cl^- on the as-formed
308 gypsum crystals precipitated in the presence of Li^+ and Mg^{2+} but only trace amount of Cl^- on
309 the gypsum crystals formed in the presence of Na^+ and K^+ . Sakuma and Kawamura (2011) used
310 molecular dynamics modelling and suggested that cations co-adsorb with chloride on
311 muscovite surfaces. In addition, Rahnemaie et al., (2006), documented that in the goethite-
312 solution double layer Cl^- was closer to the surface than the other ions, and that Li^+ and Na^+
313 were at the intermediate position of the double layer and K^+ was at the largest distance.

314 Our observations are in agreement with these previous reports for the monovalent ions Li^+ , Na^+
315 and K^+ , but we evidenced further the role of Li^+ and Mg^{2+} in co-adsorbing the chloride ion.
316 This is further supported by the fact that, neither on the surfaces of the as-formed additive-free
317 gypsum crystals nor in all the post desorption gypsum crystals Cl^- was detected by XPS (Table
318 1 and Fig. S4). This is despite the fact that in all initial solutions used for precipitating gypsum
319 crystals, calcium chloride was a major source of Cl^- in all solutions (200 mmol/L). Moreover,
320 in the samples where Li^+ and Mg^{2+} ions and chloride were determined to be adsorbed to the
321 gypsum surfaces (Table 1), the atomic percentage of the adsorbed Cl^- was in a ratio close to
322 1:1 with the adsorbed Li^+ and Mg^{2+} . This suggest that Li^+ and Mg^{2+} likely adsorbed onto the
323 gypsum surfaces as chloride ion-pairs or complexes such as $LiCl(H_2O)_4$ for Li^+ (Sobolewski &
324 Domcke, 2005) and $[MgCl(H_2O)_M]^+$ for Mg^{2+} (Siokou et al., 2003). For Li^+ this is supported
325 by the fact that the binding energies for $Li\ 1s$ and $Cl\ 2p_{3/2}$ at 55.8 eV and 198.5 eV, are the
326 same as the binding energies of these two ions in $LiCl$ (REF WILL BE INSERTED).

327 It is also worth mentioning that compared with the additive-free gypsum crystals, the Li^+ and
328 Mg^{2+} surface adsorption via sulfate binding shifted the S $2p_{3/2}$ toward higher binding energies
329 by 0.2 eV and 0.49 eV for Li^+ and Mg^{2+} , respectively (Fig. S11). This shift was not observed
330 for the adsorbed Na^+ or K^+ , which indicates their low surface adsorption. Hou et al. (2014)
331 reported S $2p_{3/2}$ binding energy variations related to Mg^{2+} association with hydrothermally
332 synthesised calcium sulfate hemihydrate crystals. They attributed this shift to the partial
333 substitution of Ca^{2+} with Mg^{2+} in the calcium sulfate hemihydrate (bassanite) structure and the
334 higher electronegativity of Mg^{2+} (1.39) with respect to Ca^{2+} (1.00), which explained the higher
335 binding energy between Mg^{2+} and S compared to those between Ca^{2+} and S.

336 Analysing the post desorption gypsum crystals revealed that only Na^+ became partly (max
337 25%) incorporated into the gypsum structure. Such an incorporation likely happened through
338 substitution of Na^+ for Ca^{2+} specially as Na^+ has the closest ionic radius (1.16 Å) to Ca^{2+} (1.12
339 Å) compared to the other studied cations ($\text{Li}^+ = 0.92$ Å, $\text{K}^+ = 1.52$ Å and $\text{Mg}^{2+} = 0.89$ Å).
340 Therefore, in gypsum it is likely that Ca^{2+} became substituted by 2 Na^+ ions with one of the
341 Na^+ ions occupying the interstitial positions in the water layer Freyer et al., 1999; Kushnir,
342 1980.

343 We are the first to show that when gypsum crystals grown in solutions containing low to high
344 concentrations of monovalent and divalent ions, the prime interaction is through adsorption
345 and that structural incorporation is only a minor effect for Na^+ . Previous studies (Kushnir,
346 1982) reported that Sr^{2+} , Mg^{2+} , Na^+ , and K^+ ions present in seawater brines became partitioned
347 into growing gypsum crystals, but no determination whether the partitioning was because of
348 the surface adsorption or structural incorporation is available. Recently, Wang and Meldrum
349 (2012) showed that gypsum crystals synthesised from experimental solutions containing 200
350 mmol/L Mg^{2+} contained a small, but measurable amount (0.4% mol) of Mg^{2+} in their structure.
351 Similarly, Ahmed et. al. (2014) suggested from XRD analysis of the shift in d-spacing of the

352 gypsum (020) peak, that Mg^{2+} become incorporated into the structure and suggested that this
353 occurred by Mg^{2+} substituting for Ca^{2+} . Based on the same approach they suggested that Na^+
354 did not incorporate into the gypsum structure (Ben Ahmed et al., 2014). In our current work,
355 although we observed a similar shift towards lower 2θ in the gypsum (020) peak position
356 as a function of Mg^{2+} concentration (Fig S12), we assert that this is more a function of inherent
357 differences in crystallization paths and not due to the presence of the magnesium ion during
358 gypsum growth. This is because we clearly documented, by two complementary approaches
359 (ICP-MS/ICP-OES analyses of pre- and post-desorption digests and XPS analyses of pre- and
360 post- desorption crystal surfaces), that only <25% of Na^+ became incorporated into the gypsum
361 structure, while all other ions, even at high concentrations, were solely adsorbed to the growing
362 gypsum crystal surfaces. There, they affected both the growth kinetics and the shapes of the
363 resulting gypsum crystals.

364

365 **4.3. Morphological modification**

366

367 The selective adsorption of additives onto the growing gypsum crystals inhibited their
368 growth along specific directions and thus modified their shapes (Fig. 4 and S5). It is not
369 surprising that such inhibition and consequent shape modifications affect most often particular
370 crystal faces and this depends on the attachment energies of the crystal faces Schmidt and
371 Ulrich, 2012. Recently, Massaro et al (2011) demonstrated theoretically that for gypsum, there
372 is a higher site density (Ca^{2+} and SO_4^{2-}) on the (021) planes compared to the fully hydrated
373 (020) planes. Furthermore, the higher surface energy of the (021) faces compared to the (020)
374 faces will affect additives adsorption more Massaro et al., 2011. This is in line with our
375 observations that show that the preferential adsorption of ions happened onto the (021) faces
376 and this favoured growth along the (020) face resulting in the preferential elongation of this

377 face (Fig 4, S5 and S13). In the presence of additives (specially Li^+ and Mg^{2+}) the resulting
378 elongated gypsum crystals was accompanied by a corresponding decrease in the crystal widths
379 (Fig 5 and S6). Furthermore, the presence of additives also affected the growth mechanisms.
380 The spiral growth we have observed for gypsum crystals grown in the presence of additives,
381 together with uneven crystal tips and the presence of growth steps on the crystal surfaces (Fig
382 6 and S7-10) also confirm the role of additives in gypsum crystal growth. Such observations
383 have not been reported before for mono and divalent ions but similar growth macro-steps have
384 been reported for gypsum crystals grown in the presence of acrylic polymers (Montagnino et
385 al., 2011).

386

387 **5. Conclusion**

388

389 With this study we have quantitatively documented the effects that alkali and alkaline earth
390 metals have on the crystallisation of gypsum. The additives increased the time needed for its
391 precipitation to be initiated in the order of $\text{K}^+ < \text{Na}^+ < \text{Li}^+ < \text{Mg}^{2+}$. In all cases, gypsum was the
392 sole precipitated phase after 200 minutes and the additives did not cause any phase
393 transformation even at high salt concentrations (500 mmol/L). The combination of ICP-MS /
394 ICP-OES of digested as-formed and post-desorbed digested gypsum crystals together with XPS
395 analyses of the surfaces of these solids revealed that Li^+ , K^+ and Mg^{2+} only adsorbed on the
396 surfaces of the gypsum crystals, while small fraction of associated Na^+ (max 25%) became
397 structurally incorporated. Growing in the presence of all additives resulted in elongated gypsum
398 crystals, with the change in aspect ratio compared to the additive free system being most
399 prominent in the presence of Li^+ and Mg^{2+} because of their higher surface adsorption affinities.

400

401 Supplementary information

402 The following materials are found in the Supplementary information: Figures S1-13 and Tables
403 S1-3.

404

405 **Acknowledgements**

406 This study was supported by a Marie Curie grant from the European Commission in the
407 framework of the MINSC ITN (Initial Training Research network), Project number 290040.

408 The authors would like to thank the Cohen Laboratories in the School of Earth and
409 Environment, and the Leeds Electron Microscopy and Spectroscopy Centre (LEMAS) for help
410 and access to instruments during the course of this study.

411

412 **References**

413

- 414 Abràmoff, M. D., Magalhães, P. J. & Ram, S. J. 2004. Image processing with ImageJ. *Biophotonics*
415 *international*, 11, 36-42.
- 416 Ben Ahmed, S., Tlili, M. M., Amami, M. & Ben Amor, M. 2014. Gypsum Precipitation Kinetics and
417 Solubility in the NaCl–MgCl₂–CaSO₄–H₂O System. *Industrial & Engineering Chemistry*
418 *Research*, 53, 9554-9560.
- 419 Bourikas, K., Hiemstra, T. & Van Riemsdijk, W. 2001. Ion pair formation and primary charging
420 behavior of titanium oxide (anatase and rutile). *Langmuir*, 17, 749-756.
- 421 Dove, P. M. & Czank, C. A. 1995. Crystal chemical controls on the dissolution kinetics of the
422 isostructural sulfates: Celestite, anglesite, and barite. *Geochimica et Cosmochimica Acta*, 59,
423 1907-1915.
- 424 Elgquist, B. & Wedborg, M. 1978. Stability constants of NaSO₄⁴⁻, MgSO₄, MgF⁺, MgCl⁺ ion pairs at
425 the ionic strength of seawater by potentiometry. *Marine Chemistry*, 6, 243-252.
- 426 Farmanesh, S., Alamani, B. G. & Rimer, J. D. 2015. Identifying alkali metal inhibitors of crystal growth:
427 a selection criterion based on ion pair hydration energy. *Chemical Communications*, 51,
428 13964-13967.
- 429 Freyer, D., Reck, G., Bremer, M. & Voigt, W. 1999. Thermal behaviour and crystal structure of
430 sodium-containing hemihydrates of calcium sulfate. *Monatshefte für Chemie/Chemical*
431 *Monthly*, 130, 1179-1193.
- 432 Gierst, L., Vandenberghe, L., Nicolas, E. & Fraboni, A. 1966. Ion pairing mechanisms in electrode
433 processes. *Journal of The Electrochemical Society*, 113, 1025-1036.
- 434 Hamdona, S. K. & Al Hadad, U. A. 2007. Crystallization of calcium sulfate dihydrate in the presence of
435 some metal ions. *Journal of Crystal Growth*, 299, 146-151.
- 436 Hasson, D., Addai-Mensah, J. & Metcalfe, J. 1990. Filterability of gypsum crystallized in phosphoric
437 acid solution in the presence of ionic impurities. *Industrial & engineering chemistry research*,
438 29, 867-875.
- 439 Hoang, T. A., Ming Ang, H. & Rohl, A. L. 2011. Investigation into the effects of phosphonic inhibitors
440 on the formation of calcium sulfate scales. *Desalination and Water Treatment*, 29, 294-301.

441 Jiang, G., Fu, H., Savino, K., Qian, J., Wu, Z. & Guan, B. 2013. Nonlattice Cation-SO₄²⁻-Ion Pairs in
442 Calcium Sulfate Hemihydrate Nucleation. *Crystal Growth & Design*, 13, 5128-5134.

443 Johnson, S. B., Scales, P. J. & Healy, T. W. 1999. The binding of monovalent electrolyte ions on α -
444 alumina. I. Electroacoustic studies at high electrolyte concentrations. *Langmuir*, 15, 2836-
445 2843.

446 Kerisit, S. & Parker, S. C. 2004. Free energy of adsorption of water and metal ions on the {1014}
447 calcite surface. *Journal of the American Chemical Society*, 126, 10152-10161.

448 Kowacz, M., Putnis, C. & Putnis, A. 2007. The effect of cation: anion ratio in solution on the
449 mechanism of barite growth at constant supersaturation: role of the desolvation process on
450 the growth kinetics. *Geochimica et Cosmochimica Acta*, 71, 5168-5179.

451 Kruger, A., Focke, W. W., Kwela, Z. & Fowles, R. 2001. Effect of ionic impurities on the crystallization
452 of gypsum in Wet-Process Phosphoric Acid. *Industrial & Engineering Chemistry Research*, 40,
453 1364-1369.

454 Kushnir, J. 1980. The coprecipitation of strontium, magnesium, sodium, potassium and chloride ions
455 with gypsum. An experimental study. *Geochimica et Cosmochimica Acta*, 44, 1471-1482.

456 Leaist, D. G. & Goldik, J. 2001. Diffusion and ion association in concentrated solutions of aqueous
457 lithium, sodium, and potassium sulfates. *Journal of solution chemistry*, 30, 103-118.

458 Mao, X., Song, X., Lu, G., Sun, Y., Xu, Y. & Yu, J. 2014. Effects of Metal Ions on Crystal Morphology
459 and Size of Calcium Sulfate Whiskers in Aqueous HCl Solutions. *Industrial & Engineering
460 Chemistry Research*, 53, 17625-17635.

461 Massaro, F. R., Rubbo, M. & Aquilano, D. 2011. Theoretical equilibrium morphology of gypsum
462 (CaSO₄·2H₂O). 2. The stepped faces of the main [001] zone. *Crystal Growth & Design*, 11,
463 1607-1614.

464 Montagnino, D., Costa, E., Massaro, F., Artioli, G. & Aquilano, D. 2011. Growth morphology of
465 gypsum in the presence of copolymers. *Crystal Research and Technology*, 46, 1010-1018.

466 Rabizadeh, T., Peacock, C. L. & Benning, L. G. 2014. Carboxylic acids: effective inhibitors for calcium
467 sulfate precipitation? *Mineralogical Magazine*, 78, 1465-1472.

468 Rahnamaie, R., Hiemstra, T. & van Riemsdijk, W. H. 2006. A new surface structural approach to ion
469 adsorption: Tracing the location of electrolyte ions. *Journal of colloid and interface science*,
470 293, 312-321.

471 Reardon, E. 1975. Dissociation constants of some monovalent sulfate ion pairs at 25. deg. from
472 stoichiometric activity coefficients. *The Journal of Physical Chemistry*, 79, 422-425.

473 Sakuma, H. & Kawamura, K. 2011. Structure and dynamics of water on Li⁺, Na⁺, K⁺, Cs⁺, H₃O⁺-
474 exchanged muscovite surfaces: a molecular dynamics study. *Geochimica et Cosmochimica
475 Acta*, 75, 63-81.

476 Sayan, P., Titiz-Sargut, S. & Avci, B. 2007. Effect of trace metals on reactive crystallization of gypsum.
477 *Crystal Research and Technology*, 42, 961-970.

478 Schmidt, C. & Ulrich, J. 2012. Morphology prediction of crystals grown in the presence of impurities
479 and solvents—an evaluation of the state of the art. *Journal of Crystal Growth*, 353, 168-173.

480 Sun, J., Wang, L. & Yu, G. 2015. Effects of Na, Ca, Mg, and Al Chloride Salts on Dissolution and Phase
481 Stability of Calcium Sulfate Dihydrate in Aqueous Solutions at 278.15 K to 308.15 K. *Journal
482 of Chemical & Engineering Data*.

483 Sverjensky, D., Shock, E. & Helgeson, H. 1997. Prediction of the thermodynamic properties of
484 aqueous metal complexes to 1000 C and 5 kb. *Geochimica et Cosmochimica Acta*, 61, 1359-
485 1412.

486 Tanji, K. K. 1969. Solubility of gypsum in aqueous electrolytes as affected by ion association and ionic
487 strengths up to 0.15 M and at 25. deg. *Environmental Science & Technology*, 3, 656-661.

488 Yang, L., Wu, Z., Guan, B., Fu, H. & Ye, Q. 2009. Growth rate of α -calcium sulfate hemihydrate in K-
489 Ca-Mg-Cl-H₂O systems at elevated temperature. *Journal of Crystal Growth*, 311, 4518-
490 4524.

491 Zhang, Y., Yang, Z., Guo, D., Geng, H. & Dong, C. 2013. Effect of chloride salts and bicarbonate on
492 solubility of CaSO₄ in aqueous solutions at 37 C. *Procedia Environmental Sciences*, 18, 84-91.
493